NANO · MICRO small
www.small-journal.com

# Nanorheology and Nanoindentation Revealed a Softening and an Increased Viscous Fluidity of Adherent Mammalian Cells upon Increasing the Frequency

*Victor G. Gisbert, Francsico M. Espinosa, Juan G. Sanchez, Maria Concepcion Serrano, and Ricardo Garcia**

**The nanomechanical response of a cell depends on the frequency at which the cell is probed. The components of the cell that contribute to this property and their interplay are not well understood. Here, two force microscopy methods are integrated to characterize the frequency and/or the velocity-dependent properties of living cells. It is shown on HeLa and fibroblasts, that cells soften and fluidize upon increasing the frequency or the velocity of the deformation. This property was independent of the type and values (25 or 1000 nm) of the deformation. At low frequencies (2-10 Hz) or velocities (1–10 µm $s^{-1}$), the response is dominated by the mechanical properties of the cell surface. At higher frequencies (>10 Hz) or velocities (>10 µm $s^{-1}$), the response is dominated by the hydrodynamic drag of the cytosol. Softening and fluidization does not seem to involve any structural remodeling. It reflects a redistribution of the applied stress between the solid and liquid-like elements of the cell as the frequency or the velocity is changed. The data indicates that the quasistatic mechanical properties of a cell featuring a cytoskeleton pathology might be mimicked by the response of a non-pathological cell which is probed at a high frequency.**

## 1. Introduction

There is a close relationship among mechanical forces, cell shape, and physiology. Cellular processes such as adhesion, motility, and growth are associated with the mechanical properties of cells and their environment.[1–3] A complete understanding of the cell mechanobiology requires the development of very sensitive and accurate high-spatial resolution methods.

Several theoretical and experimental challenges must be overcome to provide accurate and high-spatial resolution measurements of the mechanical properties of live cells.[4–7] A mammalian cell is a highly complex and organized system. The plasma membrane encapsulates a variety of solid elements and structures (cortex, cytoskeleton, molecular motors, protein fibers, DNA, organelles, nucleus) immersed in aqueous medium (cytosol). A living cell is a dynamic system that exchanges energy and matter with the environment. Its mechanical state and properties might evolve with time. In this context, it is far from surprising to find out discrepancies among the mechanical property values provided by optical, magnetic, micropipette or force microscopy (AFM) methods.[4–6]

The discrepancies were explained in terms of the different spatial and time scales probed by AFM, micropipette aspiration or magnetic twisting cytometry experiments.[4] It was also noted the physical parameters measured by the aforementioned methods were not equivalent.[4–6] This context is slowing down the development of a comprehensive description of the mechanical properties of single cells. Specifically, the measurements have not clarified the interplay between the solid and liquid elements in regulating the mechanical response to a deformation. At a fundamental level, the use of different mechanical parameters such as storage and loss moduli in rheology or elastic modulus and viscosity coefficients in AFM-based indentation, has obscured the understanding of the cell frequency and/or velocity-dependent behaviors.

In the last few years, advances in force microscopy instrumentation and standardization[7–19] have led to several breakthroughs in cell nanomechanics. High-spatial resolution measurements of intracellular forces,[7–8] imaging of subsurface structures,[9] high-frequency,[13] or high-speed images,[19] were reported. The experimental activity motivated the development of several models, methods and simulations to transform AFM observables into elastic and viscoelastic properties.[20–35] The overall activity has led to the consolidation of a mammalian cell as a complex

V. G. Gisbert, F. M. Espinosa, J. G. Sanchez, M. C. Serrano, R. Garcia
Instituto de Ciencia de Materiales de Madrid
CSIC
c/ Sor Juana Inés de la Cruz 3, Madrid 28049, Spain
E-mail: r.garcia@csic.es

The ORCID identification number(s) for the author(s) of this article can be found under https://doi.org/10.1002/smll.202304884



**DOI: 10.1002/smll.202304884**

viscoelastic system.[4,6–7] It has also strengthened the applications of AFM in mechanobiology.[36–40]

Several AFM-based methods such as force-distance curves (constant velocity),[7] oscillatory indentation (sinusoidal velocity),[13,40] multifrequency,[12] load relaxation and creep measurements[33–34] have been applied to study cells. Force-distance curves (FDC) and its extension to generate nanomechanical maps (force-volume) are implemented in most commercial AFMs. For that reason, FDCs are widely applied to characterize single cells. On the other hand, oscillatory indentation experiments provided a simplified transformation between AFM observables and storage and loss moduli which made them easy to interpret. In what follows, nanoindentation refers to experiments performed at constant velocity while nanorheology refers to experiments performed with a sinusoidal velocity.

Here, we integrate nanorheology, nanoindentation, and theory to provide a unified description of the velocity and frequency dependencies of the mechanical properties of a mammalian cell. Nanorheology and nanoindentation experiments show similar frequency and velocity-dependent properties. Adherent cells become softer and more liquid-like if they are deformed at moderate to high frequencies or velocities. Softening meant lower scaling modulus values while an increase of the liquid-like behavior was associated with higher values of the fluidity coefficient. The above findings were verified on HeLa and fibroblasts NIH 3T3 cells over a wide range of velocities (1-300 μm $s^{-1}$) and frequencies (1-1100 Hz).

Frequency-dependent experiments were performed on HeLa cells exposed to a drug that disrupted F-actin polymerization. A comparison between the frequency response of treated and untreated cells shows that the mechanical properties of pathological cells might be mimicked by the response of non-pathological cells if the measurements are performed at a high frequency.

The time-dependent response of an adherent cell reflects the interplay between the cell surface (solid-like) and cytosol (liquid-like). At low velocities or frequencies, the cell viscoelastic response was dominated by interactions happening at the cell surface (plasma membrane and cortex). At high velocities (frequencies), the viscoelastic response was dominated by the hydrodynamic drag of the cytosol. The trends observed as a function of the frequency, specifically, the decrease of the scaling modulus and the increase of the fluidity coefficient, were independent of the deformation range (from 25 to 1000 nm).

The softening and fluidization of a mammalian cell as the frequency is increased does not seem to involve any structural remodeling of the cell. It is interpreted as a redistribution of the mechanical stress between the solid and liquid components of the cell. The liquid-like response becomes more relevant from moderate to high frequencies or velocities.

## 2. Results and Discussion

### 2.1. Overview Experimental Data in Nanoindentation and Nanorheology

**Figure 1** shows AFM nanomechanical and confocal microscopy images of HeLa cells. The AFM map (Figure 1a) combines different nanomechanical signals (topography and fluidity coefficient). It has been shown that the combination of different nanomechanical signals in a single image enhances the contrast and the spatial resolution of AFM.[9] Specifically, the AFM image reveals several elements of the cell cytoskeleton architecture and the nucleus (Figure 1a). The confocal microscopy image provides information on the cell's height at zero force (Figure 1b). The cell's height is needed as an input to modeling the cell mechanical response. Representative force-indentation curves obtained on a HeLa cell by, respectively, nanoindentation (Figure 1c) and nanorheology (Figure 1d) are shown. The hysteresis of those curves revealed the existence of energy dissipation processes within the cell. Examples of the indentation signals (Figure 1f) and time-varying forces (Figure 1e) are also shown.

### 2.2. Theory

A two-step process is followed to link the AFM observables to mechanical properties. First, the cell viscoelastic response (relaxation function) was defined. Second, a contact mechanics model was implemented to describe the tip-cell contact area as a function of the indentation.

### 2.3. Three-Dimensional Power-Law Viscoelastic Model

Several viscoelastic models were applied to determine mechanical properties of soft matter from AFM experiments.[6,7,23,25,27,31] In particular, power-law rheology models were applied to describe the mechanical properties of cells.[2,26,42–44] It was shown that some power-law rheology models provided a more efficient description of the cell response than linear viscoelastic models based on mechanical analogs.[42] We implemented a single power-law rheology model that expressed the relaxation modulus of the cell in terms of two parameters,[32] scaling modulus and fluidity coefficient. In this model the relaxation function is given by[45]

$$E = \frac{E_0}{\Gamma(1-\gamma)}\left(\frac{t}{t_0}\right)^{-\gamma} \quad (1)$$

where Γ is the gamma function; $E_0$ is a scaling factor with units of force divided by area (scaling modulus). It has been identified as the elastic modulus of the material at time $t_0$ (commonly $t_0$ = 1 s). The exponent $\gamma$ captures the dissipative effects happening in the material during the deformation (fluidity coefficient). A value $\gamma = 0$ defines an elastic solid of Young's modulus $E_0$ while a $\gamma = 1$ indicates a Newtonian viscous liquid.

The contact mechanics model is derived by applying the correspondence elastic-viscoelastic principle[46] and Ting's solution[47] to describe the contact area during retraction. In this model, an integral equation links the viscoelastic model, the contact area and the applied force. To find the analytical solutions to the above integral equation has been a challenge.[31–32]

### 2.4. Theoretical Expression of the Force in Nanoindentation

In a nanoindentation experiment, a cell is deformed at constant speed by applying a triangular waveform signal to the

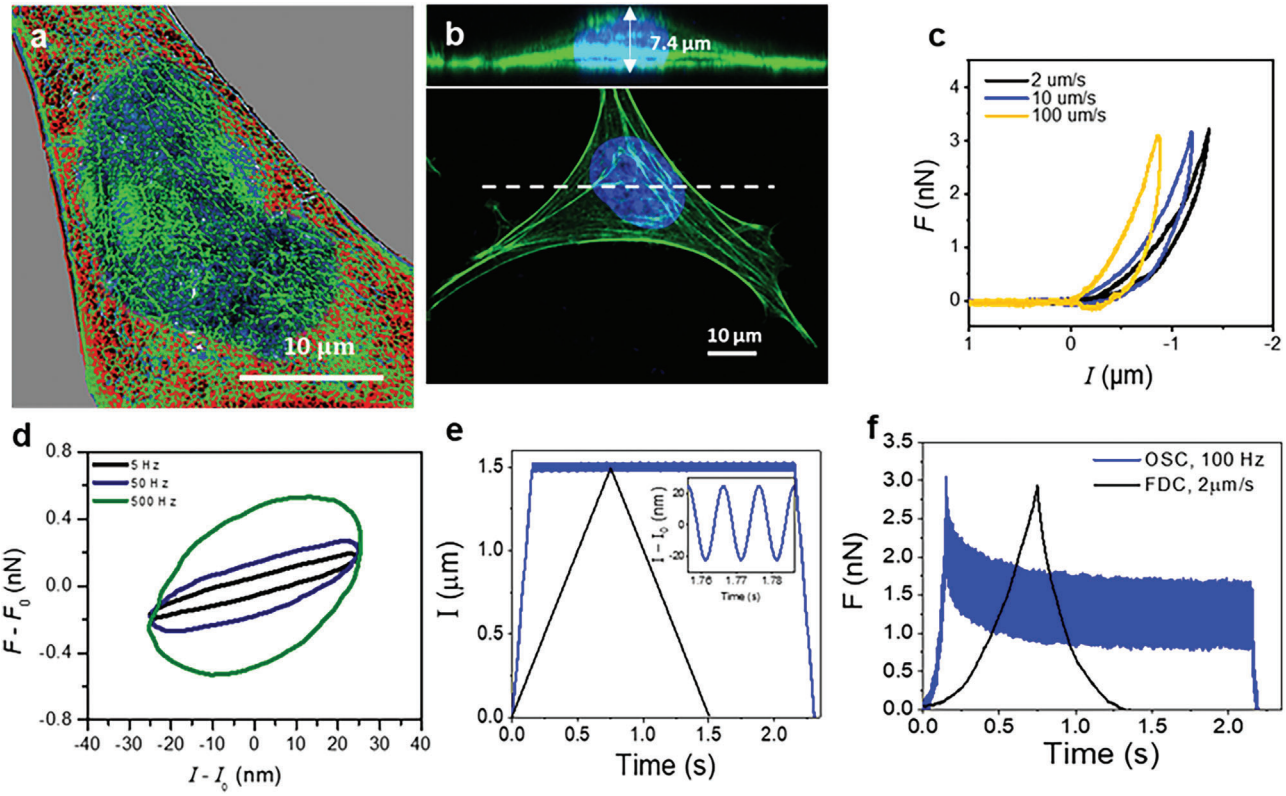


**Figure 1.** Schemes of the nanorheology and nanoindentation experiments on cells. a) Hybrid AFM image. The image combines topography, modulus, and fluidity images. The color scale is arbitrary because the image combines data with different magnitudes. b) Confocal microscopy images. Top, lateral cross-section. Bottom, plane view. The dashed line indicates the position at which the lateral cross-section intersected the plane view image. Actin filaments and nuclear DNA were labeled, respectively, in green and blue (see Section S9, Supporting Information). c) Examples of force-distance curves (nanoindentation) obtained on a HeLa cell at three velocities. d) Examples of oscillatory force-distance curves (nanorheology) obtained on a HeLa cell at three frequencies. e) Examples of indentation versus time curves obtained in nanoindentation ($v = 2$ µm s$^{-1}$, in black) and nanorheology ($f = 100$ Hz, in blue). f) Force-time curves in nanorheology ($f = 100$ Hz, blue) and nanoindentation ($v = 2$ um s$^{-1}$, black). The curves correspond to the indentations depicted in (e). Panels (a) and (b) correspond to different HeLa cells in similar metabolic states. The hysteresis loops observed in (c) and (d) indicated the presence of viscoelastic processes. Parameters, $k = 0.21$ N m$^{-1}$, $Q = 1.97$, $f_o = 121$ kHz.

z-displacement. At the same time, the force is measured as a function of time or distance. The representation of the force as a function of the distance is commonly called a force-distance curve (FDC).[7] To transform a FDC generated with a triangular waveform (Figure 1e) into material properties require two main steps. First, to convert the primary observables (deflections and *z*-piezo displacements) into forces and cell deformations. This step has been extensively discussed.[7,48] Second, to transform the forces and deformations into mechanical properties. This step involved the implementation of a constitutive model for the cell's relaxation function together with a contact mechanics model for determining the tip-cell contact area. The latter should take into account the finite-thickness of the cell and the history of the deformation. All those features were considered to deduce an analytical expression for the force exerted by a conical tip that indents ($I$) a cell at a constant speed,[32,44]

$$F_{\text{semi}}(t) = \begin{cases} \frac{16\tan\theta}{3\pi} \times \frac{E_0}{\Gamma(3-\gamma)} I^2 \left(\frac{t}{t_0}\right)^{-\gamma} & t \le t_{\max} \\ \frac{16\tan\theta E_0 t_0^{\gamma} v_0^2}{3\pi\Gamma(1-\gamma)} \times \frac{t^2\left(\left(1-\frac{t_1}{t}\right)^{\gamma}-1\right)+\gamma t_1 t-(\gamma-1)t_1^2}{(t-t_1)^{\gamma}(\gamma-2)(\gamma-1)} & t > t_{\max} \end{cases} \quad (2)$$

where $t_1$ is defined by

$$t_1(t) = t - \sqrt[1-\gamma]{1 + \frac{v_{ret}}{v_{app}}}\left(t - t_{\max}\right) \quad (3)$$

where $F_{semi}$ is the force exerted on a sample of semi-infinite thickness which has the same power-law parameters than the real cell; $h$ is the cell thickness. The above expressions assumed a Poisson ratio of 0.5. The experiments were performed by using sharp probes ($\theta \le 18°$) and low to moderate indentations ($I/h \le 20\%$). We verified that under the above conditions, bottom-effect corrections[31–32] were negligible, therefore,

$$F(t) = F_{\text{cell}}(t) \approx F_{\text{semi}}(t) \quad (4)$$

The above expression reproduced the experimental force-distance curves obtained on HeLa and fibroblast cells.[44]

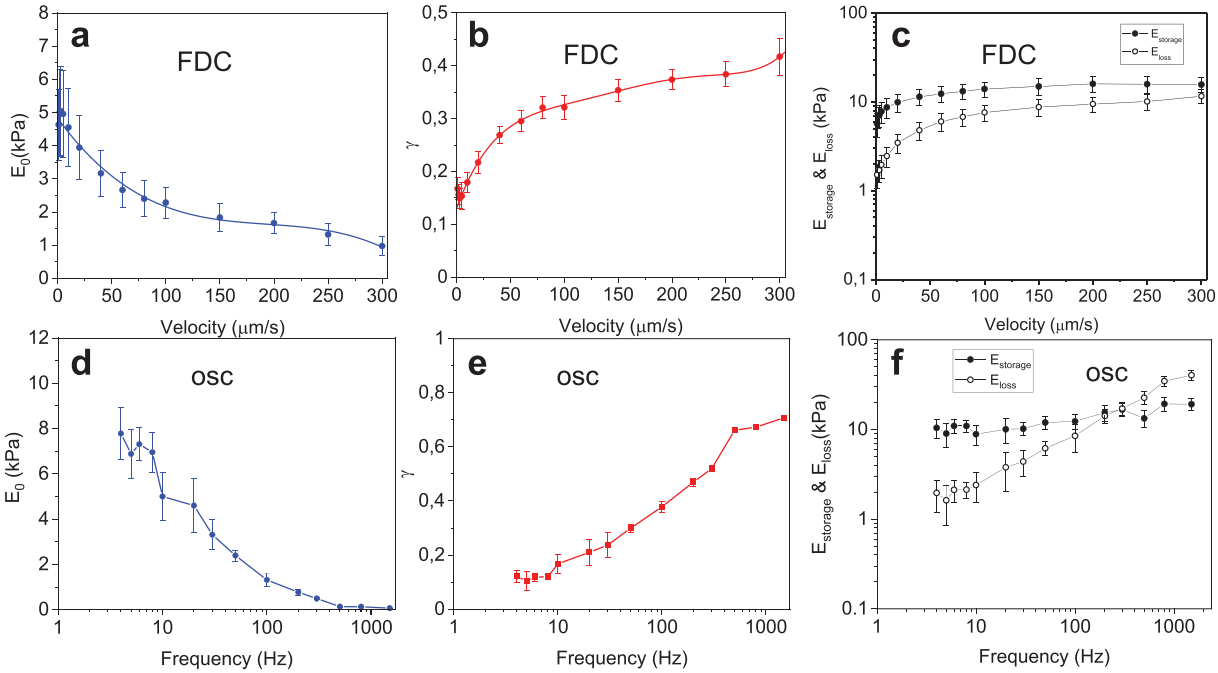


**Figure 2.** Power-law rheology parameters from FDC and oscillatory experiments. a) Scaling modulus as a function of the indentation velocity (FDC). b) Fluidity coefficient (FDC). c) Storage and loss modulus (FDC). d) Scaling modulus (osc). e) Fluidity coefficient (osc). f) Storage and loss moduli (osc). Measurements performed on the same HeLa cell. Microcantilever, FDC and oscillatory parameters, $k = 0.21$ N m$^{-1}$, $Q = 1.97$, $f_o = 121$ kHz; $F_{max} = 3$ nN, $I_{max} = 1$-1.5 μm (FDC); $I_0 = 1$ μm; $I_{osc} = 25$ nm, $n_{FDC} = 72$, $n_{osc} = 36$.

### 2.5. Theoretical Expression of the Force in Nanorheology

The use of sinusoidal waveforms to determine the mechanical properties of cells constitutes the basis of rheology either at macro, micro and nanoscale domains. Oscillatory measurements involve an initial step deformation $I_0$ which is followed by a sinusoidal deformation. Typical $I_0$ values were of 1000 nm while the amplitude of the oscillation was of 25 nm. The tip remains in contact with the cell during the whole oscillation cycle. For small amplitude indentations with respect to $I_0$, a Taylor expansion gives

$$F(t) - F_0 \approx \alpha \cdot \beta \cdot I_0^{\beta-1} \cdot E^*(t) \cdot \left(I(t) - I_0\right) \quad (5)$$

$$I(t) = I_0 + I_{osc} \cos \omega t \quad (6)$$

where $\alpha$ is a parameter that depends on the geometry of the probe and the Poisson ratio; $\beta$ is a coefficient that depends on the geometry. The complex relaxation modulus $E^*$ of the cell subjected to a periodic deformation of angular frequency $\omega$ was given by[49]

$$E^*(\omega) = E_0 \left(\frac{\omega}{\omega_0}\right)^{\gamma} \left[\cos\left(\frac{\pi}{2}\gamma\right) + i \sin\left(\frac{\pi}{2}\gamma\right)\right] = E_{storage} + iE_{loss} \quad (7)$$

where $\omega_0 = 1$ rad s$^{-1}$. In the frequency domain, the relationship between the complex modulus and the force was given by[50]

$$E^*(\omega) = \frac{\pi\left(1-\nu^2\right)}{4 I_0 \tan\theta} \left[\frac{F(\omega)}{I(\omega)} e^{i\varphi} - i\omega b\right] \quad (8)$$

where $\varphi$ is the phase delay[13,49] and $b$ is the coefficient of the hydrodynamic drag force acting on the cantilever body.[49] This coefficient should be measured near the cell surface. For nanorheology measurements, we assume that the contact area does not change within an oscillation cycle. This assumption is based on the small value of the indentation amplitude (25 nm) with respect to the step deformation ($I_0 \approx 1000$ nm).

### 2.6. Nanoindentation Data on HeLa Cells

**Figure 2**a-c shows the scaling modulus, fluidity coefficient, storage, and loss moduli of a HeLa cell as a function of the velocity of the probe. The measurements are performed by applying a maximum force of 3 nN. The force is applied on a region located above the nuclear region. The scaling modulus decreases while the fluidity increases by increasing the velocity. Specifically, the scaling modulus decreased from 5.7 kPa at 5 μm s$^{-1}$ to 600 Pa at 300 μm s$^{-1}$ (Figure 2a). The fluidity coefficient showed a monotonically increase from 0.14 (5 μm s$^{-1}$) to 0.43 (300 μm s$^{-1}$) (Figure 2b). The storage and loss moduli increase by increasing the frequency (Figure 2c). The storage and loss moduli of the cell are determined by using Equation 7. The cell's nanomechanical parameters (scaling modulus, fluidity coefficient) and the equivalent frequency are determined from a FDC experiment.

### 2.7. Nanorheology Data on HeLa Cells

Figure 2d–f depicts the scaling modulus, fluidity coefficient, storage, and loss moduli of a HeLa cell measured as a function of the

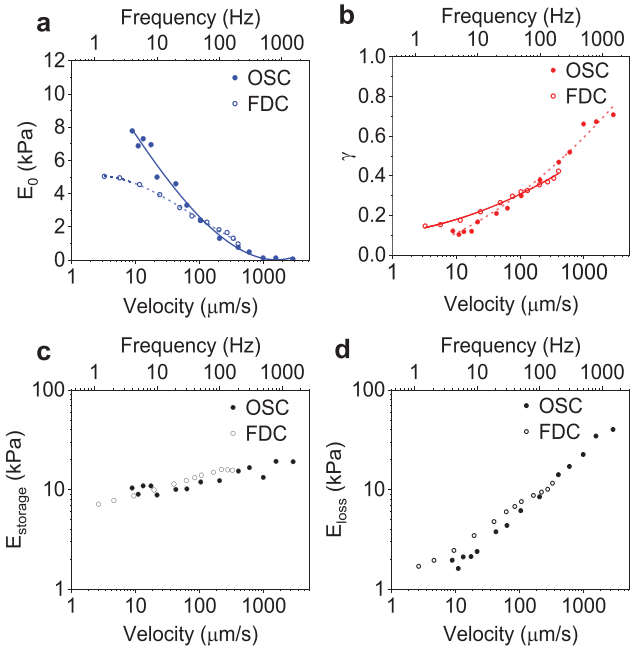


**Figure 3.** Nanoindentation (FDC) and nanorheology (osc). a) Scaling modulus. b) Fluidity coefficient. c) Storage modulus. d) Loss modulus. Data from Figure 2. The frequency axis refers to both FDC and oscillatory data. The velocity axis just applies to FDC Continuous and dashed lines were plotted to guide the eye.

frequency. The scaling modulus decreased from 7.7 kPa at 3 Hz to 200 Pa at 1100 Hz (Figure 2d). The fluidity coefficient increased from 0.1 (3 Hz) to 0.7 (1100 Hz) (Figure 2e). The storage and loss moduli increased by increasing the frequency (Figure 2f). For low to moderate frequencies (3-200 Hz), the storage modulus had larger values. A cross-over was observed at about 200 Hz.

Similar dependencies with the frequency were reported for the storage and loss moduli.[14,26,43] The cross-over between the storage and the loss moduli has been observed before on many types of mammalian cells such as fibroblasts,[13] Hela cells,[14] retinal pigmented epithelium cells[34] or kidney epithelial cells.[26,43]

### 2.8. Comparison of Nanoindentation and Nanorheology Data

**Figure 3** compares the viscoelastic parameters obtained from FDC and oscillatory measurements. The equivalent frequency of a FDC is determined from the time the tip is in contact with the cell $t_c$,

$$f = \frac{1}{t_c} = \frac{v}{2I_{max}} \tag{9}$$

Two results stand out from Figure 3. First, both methods reported the same frequency-dependent behavior. The scaling modulus decreases and the fluidity coefficient increases as the velocity (frequency) of the deformation was increased. Second, FDC and oscillatory measurements gave similar values for the fluidity coefficient, storage, and loss moduli over the whole frequency (velocity) range. The agreement was less satisfactory for the scaling modulus in the low-to-moderate frequency (velocity) range. At 9 μm $s^{-1}$ or 3 Hz the modulus measured by nanoindentation (5 kPa) was significantly smaller than the one obtained by nanorheology (8 kPa). The numerical discrepancies might be attributed to the differences in the $z$ displacement ranges of nanorheology (25 nm) and nanoindentation (1-1.5 μm). We performed similar experiments on fibroblasts (Figure S3, Supporting Information). The data reproduced point-by-point the findings obtained on HeLa cells. The reproducibility observed across two different cell lines suggested a general property.

### 2.9. Experimental Validation of the Methodology

To validate the methodology, we have thoroughly calibrated the experimental set-up. In addition, we have performed experiments on an elastic material.

The measurement and interpretation of the mechanical properties of single cells might be complicated by the existence of systematic errors. Hysteresis and creep from the $z$-piezo displacement might be wrongly interpreted in terms of cell viscoelastic properties. The hydrodynamic drag associated with the displacement of the cantilever might also introduce dissipation. This effect should affect more nanoindentation experiments. The cantilever-tip displacement in nanoindentation experiments was about 20 to 50 larger than in nanorheology. The contact mechanics model used to transform observables into mechanical parameters might be a source of systematic errors in frequency-dependent measurements. Some of those factors, in particular the influence of the hydrodynamic drag, were discussed by others.[13,48,49] Our experience indicated that to suppress or minimize errors associated with the aforementioned factors demanded an exhaustive testing of the experimental system (Figure S2, Supporting Information).

The frequency or velocity-dependent response of the power-law rheology parameters of an elastic material can be predicted. The scaling modulus should be independent on the frequency or velocity of the force-distance curves. The fluidity coefficient should be zero.

Polyacrylamide gels behave as elastic materials at low-to-moderate frequencies. The composition and cross-linking degree of the gel might be tuned to obtain a material with a stiffness comparable to those of HeLa, fibroblasts and other mammalian cells.[51] The approach and retraction sections of FDC curves obtained in the 0.5-10 μm $s^{-1}$ range showed good overlaps (**Figure 4**a,b). In fact, the average energy dissipated by the tip (per cycle) in the gel was less than 1% of the work done on the gel. The differences observed between approach and retraction were associated with the adhesion force between the tip and gel. Similarly, there was little hysteresis in the oscillatory force-distance curve (Figure 4b). Those features supported the consideration of those gels as effective elastic materials.

Figure 4c,d shows the scaling modulus and fluidity coefficient of the gel. Nanorheology and nanoindentation provided similar values for the scaling modulus (~9.5 kPa) in the 1–10 Hz or 1–10 μm $s^{-1}$ ranges. A small decrease (≤ 10%) was observed in the 1–5 Hz (1-5 μm $s^{-1}$) range. The fluidity coefficient values were extremely small (≤ 0.02) and very close to the value of an ideal elastic solid ($\gamma = 0$).

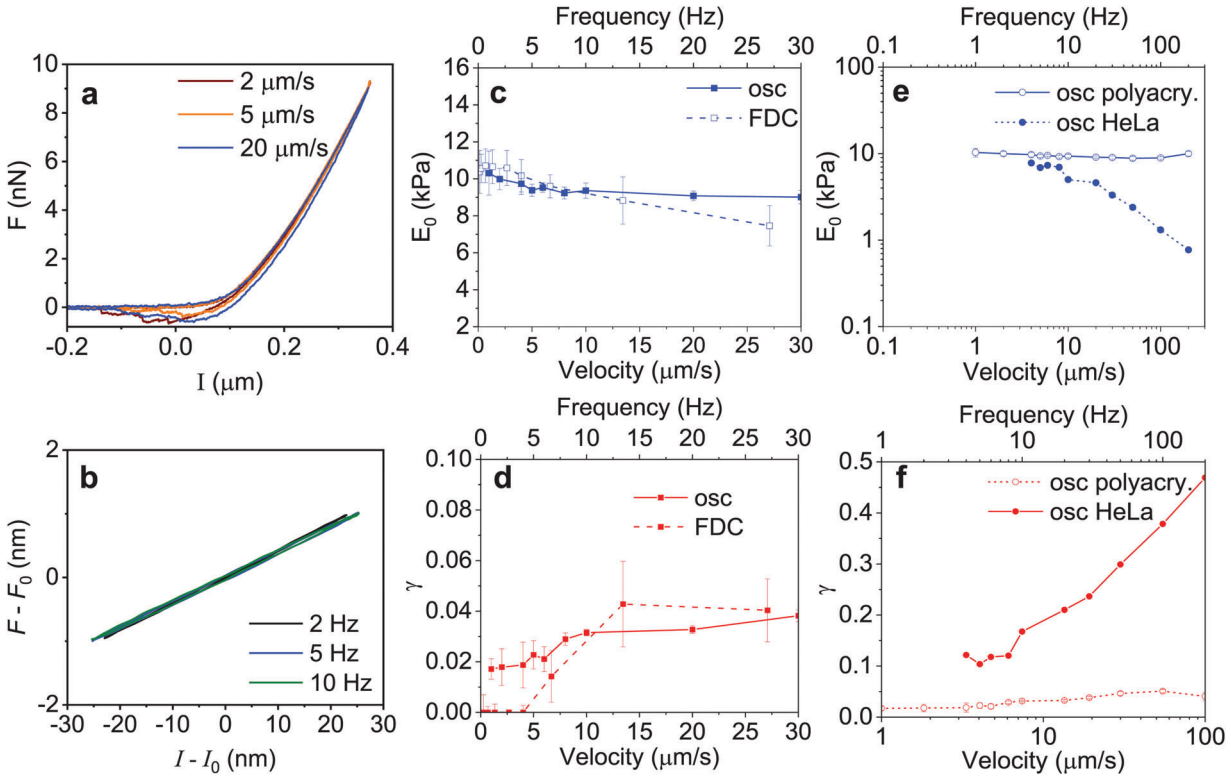


**Figure 4.** Nanorheology and nanoindentation on polyacrylamide. a) Force-distance curves in a nanoindentation experiment. In the repulsive region, the overlap between approach and retraction for a single velocity (2, 5, and 20 μm $s^{-1}$) is near perfect. This indicates the elastic character of the polyacrylamide. The adhesion forces produced some hysteresis. b) Force-distance curve in a nanorheology experiment (2, 5, and 10 Hz). The width of the loop is very small or negligible (no hysteresis). c) Scaling modulus. d) Fluidity coefficient values are very small. Those values underline the elastic behaviour of the polyacrylamide in the 1-30 Hz range. e) Scaling modulus for a Hela cell and a polyacrylamide gel. f) Fluidity coefficient for Hela and polyacrylamide. Microcantilever parameters, $R_{tip}$= 3.31 μm; $k$ = 0.08 N $m^{-1}$, $Q$=2.0, $f_o$= 4.0 kHz, $F_{max}$= 6.9 nN; $I_0$= 260 nm, $I_{osc}$= 25 nm, $n$ = 12.

Next, we compared the scaling modulus and fluidity coefficients of a HeLa cell and a polyacrylamide gel. The fluidity coefficient of the cell was about 10 times higher. In addition, the scaling modulus of the cell decreased by increasing the frequency or velocity while the one of the gel remained nearly constant (≤ 10%). This comparison provides two conclusions. First, the experimental methodology which included the 3D power-law model reproduces the expected behavior of an elastic material. Second, it provides a quantitative range for the fluidity coefficient of a material to be considered as elastic (≤ 0.05).

### 2.10. Frequency Dependency of Cells Modified by a Biochemical Drug

It is known that cytochalasin D (Cyto-D) disrupts the polymerization of F-actin. Inhibition of actin polymerization weakens the cell's cortex. AFM nanomechanical measurements showed that cells treated with Cyto-D were softer (smaller Young's modulus) than their untreated counterparts.[20,53–55]

**Figure 5**a,b compares the viscoelastic parameters obtained from a nanoindentation experiment performed on a HeLa cell before and after being treated with Cyto-D. Cells exposed to Cyto-D are softer and more liquid-like than untreated cells. Specifically, for each frequency, the modulus of treated cells is smaller. For low frequencies (≤10 Hz), the moduli of treated cells were about 2-fold smaller. The relative difference between the values of treated and untreated cells decreases as the frequency is increased. In the 1 to 200 Hz range, the fluidity coefficient of a treated cell is higher than the one of an untreated cell. Similar tendencies are found on nanorheology measurements (Figure 5c,d).

The comparison between the quasistatic or DC (≤2 Hz) nanomechanical parameters of treated (pathological) and untreated cells revealed that the DC values of a pathological cell were similar to the values measured on a non-pathological cell at a higher frequency. For example, the DC modulus of a treated cell (≈3.5 kPa) might be obtained by exciting an untreated cell to 40 Hz (Figure 5a). The DC fluidity coefficient value of a treated cell was ≈0.3. This value might be obtained by probing an untreated cell to 100 Hz (Figure 5b,d).

### 2.11. Discussion

The viscoelastic response of living cells might involve different processes. Namely solid-solid and solid-liquid interactions. The former is associated with the binding/unbinding of cross-links among protein fibers.[5,56] The latter (solid-liquid interactions) might be divided in two groups. One group is associated with the hydrodynamic squeezing of the liquid through the nanopores

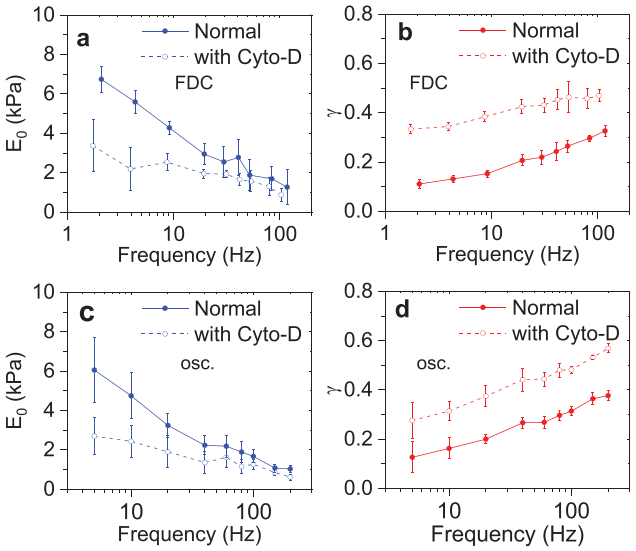


**Figure 5.** Frequency response of HeLa cells treated with Cythocalasin-D. a) Scaling modulus (nanoindentation). b) Fluidity coefficient measured (nanoindentation). c) Scaling modulus (nanorheology). d) Fluidity coefficient (nanorheology). For each method, the data show the nanomechanical values obtained on the same cell before and after exposition to Cyto-D for 30 min. Continuous and dashed lines were plotted to guide the eye. Microcantilever, FDC and oscillatory parameters, $k = 0.19$ N m$^{-1}$, $Q = 2.1$, $f_o = 130$ kHz; $F_{max} = 3$ nN, $I_{max} = 1$-2 µm (FDC); $I_{max} = 1$ µm, $I_{osc} = 12$ nm, $n = 10$.

or micropores formed by some inner cell structures.[57] The other process accounts for the hydrodynamic friction associated with the displacement of solid bodies within the cytosol or nucleosol.[9] Solid-solid and solid-liquid viscoelastic interactions might contribute simultaneously to the force measured by the AFM probe. Therefore, it

is not straightforward to separate them in a single frequency (speed) AFM measurement.

The softening and increased fluidity of cells upon an increase of the frequency or velocity of the external force underlines the interplay between the solid and liquid components, namely the cell surface and the cytosol. At low frequencies (1-20 Hz) or velocities (2-20 µm s$^{-1}$), the scaling modulus values measured by nanorheology are significantly larger than those measured by nanoindentation. The values obtained are higher because the amplitude of the deformation (25 nm) is smaller than the cortex thickness (≈150 nm). In addition, the amplitude used in nanorheology (25 nm) is smaller than the values used in nanoindentation experiments (≈1000 nm). The nanoindentation experiments involved major displacements of the cortex and cytosol. At the same time, the fluidity coefficient values reported by both methods are in the 0.1–0.2 range. Those values, albeit small, are ≈5–10 higher than the ones measured in an elastic material (Figure 4f). Altogether, the results obtained at low frequencies or velocities indicate that the mechanical response of HeLa and fibroblast cells is dominated by the properties of the plasma membrane and the cortex with some minor contribution from the cytosol.

The fluid-like behavior of a cell is enhanced by increasing the frequency or velocity of the deformation. The process leads to fluidity coefficient values ($\gamma \geq 0.7$) which are close to the one of a Newtonian liquid ($\gamma = 1$) (Figure 3b). At the same time, the scaling modulus decreases by one order of magnitude. The process is reversible. By reducing the frequency or velocity of the deformation, the modulus increases, and the fluidity coefficient is reduced. Taken together, those results suggest the absence of structural remodeling processes upon changes in the frequency or velocity of the deformation. Therefore, the changes observed in the mechanical properties should be associated with the liquid component of the cell (cytosol). We remark that softening and fluidization upon increasing the frequency or velocity of the deformation is compatible with an increase in the storage and loss moduli values (Figure 3). The above data was obtained on regions located above the nucleus. We note that preliminary experiments performed on perinuclear regions of the cell reproduced the behavior observed over nuclear regions.

Nanoindentation and nanorheology experiments were performed with cells treated with cytochalasin D (Figure 5). Those cells are softer and more liquid-like than untreated cells. The comparison between the frequency response of untreated and treated cells shows that the biochemical treatment anticipates the softening and fluidization features observed in untreated cells at high frequencies. Those findings indicate a way to mimic the mechanical response of pathological cells by performing experiments on nonpathological counterparts.

Any external force (stress) applied to a mammalian cell is distributed asymmetrically between its solid and liquid elements. The distribution depended on the frequency or velocity of the deformation. The role of the cytosol in controlling the mechanical response was enhanced by applying higher frequencies (**Figure 6**). In the present study, we have not considered explicitly the role of the nucleus on the above behavior.

Many AFM-based studies were aimed to link nanomechanical state and physiology.[38–40,58–60] In general, the results were interpreted in terms of changes happened at the cortex (solid element). Our findings do not necessarily invalidate the conclusions from those studies. Our findings indicate that the use of mechanical forces of low frequencies or velocities will minimize the coupling between the cell surface and cytosol. As a consequence, the mechanical response will be more sensitive to the structural properties of the cell surface (plasma and cortex).

## 3. Conclusion

Nanorheology, nanoindentation, and theory are integrated into an AFM methodology to characterize time-dependent properties. Nanorheology and nanoindentation experiments are performed on the same cell by using the same AFM tip. Both methods elicited similar responses over large velocity (1-300 µm s$^{-1}$) or frequency (1-1100 Hz) ranges. HeLa and NIH 3T3 cells softened and increased their viscous response upon increasing the frequency or speed at which they are deformed. The trend is independent of deformation value (25 nm or 1000 nm).

The lowest fluidity coefficient measured on a HeLa or NIH 3T3 cell ($\gamma = 0.1$) is obtained at small velocities or low frequencies. That value ≈20 times larger than the instrument noise level. This result indicates that viscous processes contribute to the mechanical response of a mammalian cell regardless of the frequency or velocity of the deformation.

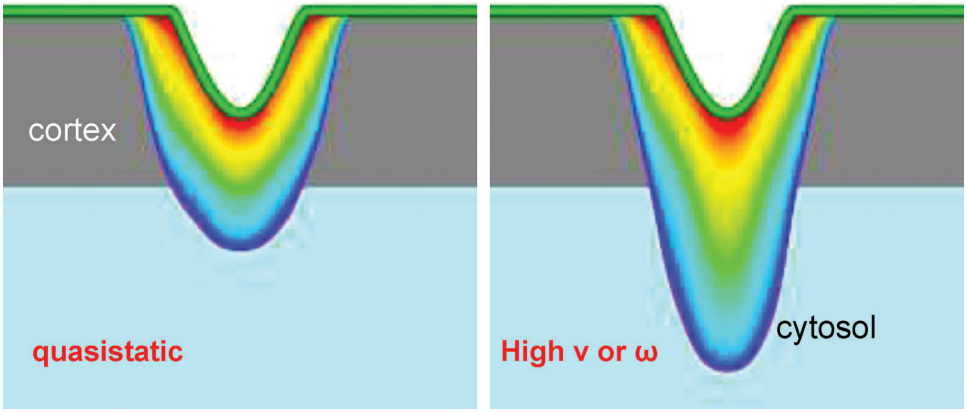


**Figure 6.** Scheme of cortex and cytosol contributions to the mechanical properties. At low frequencies or velocities, the response to a deformation is carried by the cell surface with minor contributions from the cytosol. At higher frequencies, the viscous properties of the cytosol are enhanced.

The softening and increased viscous fluidization of cells upon increasing the velocity or frequency indicates an interplay between solid (cell surface) and liquid-like elements (cytosol). Those contributions are in general intertwined. The ratio between cell surface and cytosol contributions depend on the frequency or velocity at which a cell is deformed. In the quasistatic regime, the cell surface (membrane and cortex) dominates the mechanical response. At higher frequencies or velocities (≥10 Hz; ≥10 μm $s^{-1}$), the cytosol exerts a significant influence on the mechanical properties of the cell.

The experiments performed on cells bearing a F-actin polymerization pathology show that the quasistatic response of those cells might be mimicked by measuring the properties of nonpathological cells at high frequencies.

These findings provide the most fundamental description of the mechanical response of a mammalian cell as a function of the frequency or velocity of the deformation. Any mechanobiology analysis of a cell as a function of a mechanical stimulus should explicitly consider the interplay between the solid and the liquid-like components of the cell.

## 4. Experimental Section

*Cell Types and Culture*: HeLa cells (Sigma–Aldrich) were cultured in Eagle's minimum essential medium (EMEM) with 10% calf serum-CS (Gibco Life Technologies), 1% penicillin/streptomycin (Gibco Life Technologies, UK) and 2 mM l-glutamine (Sigma–Aldrich, Missouri, USA). The cells were maintained at 37 °C under a controlled atmosphere with 90% humidity and 5% of $CO_2$. The cells were seeded in Petri dishes for 24–48 h in the culture medium before the measurements. The AFM measurements were performed in the above Petri dishes and culture medium.

*Polyacrylamide Gel*: The gel solution was prepared by mixing 40% acrylamide and 2% bisacrylamide in ultrapure water (MilliQ systems, Molsheim, France). Finally, ammonium persulfate (APS) and N, N, N', N'-Tetramethylethylenediamine (TEMED) were added to activate the polymerization. All reagents were purchased from Sigma-Aldrich.

*Cytochalasin D*: Cytochalasin D was used to test the effect of an actin filament depolymerization drug on the frequency response of cells. HeLa Cells were treated with a 5 μM concentration of cytochalasin D (Sigma–Aldrich) for 30 min at 37°. Nanoindentation and nanorheology experiments were performed immediately afterwards.

*AFM Nanoindentation and Nanorheology*: The experiments were performed with a JPK NanoWizard 3 platform (JPK Instruments AG, Berlin, Germany). The oscillatory signals for nanorheology were performed with an external generator (see below). Home-made codes were developed to process the AFM data.

FDC and nanorheology experiments on cells were obtained with Fastscan-D microcantilevers (Bruker). Those cantilevers have a pyramidal tip with an aperture semi angle of 18°. The nominal tip radius and length were, respectively, 5 nm and 3 μm. The microcantilever force constant $k$ was calibrated by using the thermal noise method. Specifically, the FDC data shown in the main text were obtained with $k = 0.21$ N $m^{-1}$. The resonant frequency as measured in the buffer was $f_0 = 121.2$ kHz. Nanoindentation and nanorheology measurements were performed with the same tip on the same central region (over the nucleus) of a single cell. Typically, the sequence was FDC and then oscillatory.

FDCs were obtained on 6 different positions located over the nucleus, 10 FDCs were obtained on each position. First, the mean value of the PLR parameters on each position is determined. Second, the mean value from those values and the associated standard deviations were determined. More information on the cell statistics is founded in Figure S2, Supporting Information.

The FDCs were obtained using a triangular waveform at 1, 2, 5,10, 20, 40, 60, 80, 100, 150, 200, 250, and 300 μm $s^{-1}$. The indentation was stopped when the force reached a value of 3 nN. The $z$-displacement was performed with a closed-loop feedback and involved a $z$-displacement of 5 μm (sampling rate of 500 data points per μm). Hence, each FDC involved 5000 data points, split in 2500 for the approach and 2500 for the retraction. The fittings were performed by applying a correlation coefficient $R$ above 0.95.

Nanorheology oscillations were generated with a signal produced by a high-frequency function generator (AFG-21105, RS PRO, UK). The oscillatory signal was added to a step signal. The step signal was generated by approaching the tip with a triangular waveform ($v = 10$ μm $s^{-1}$) to reach a peak force of 3 nN. The step indentation was in the 1-1.5 μm range. An oscillatory deformation of 50 nm (peak-to-peak) was applied during the dwell time (2 s) of the step deformation. The data from the last second was processed to deduce the parameters.

Nanoindentation and nanorheology experiments performed on polyacrylamide gels did not require sharp tips. Those measurements were performed by using spherical probes (CP-PNP-SiO-C, diameter 6.62 μm, NanoAndMore).

*Additional Theory to Process FDC and Oscillatory Data*: Two different expressions were needed to determine force as a function of time, one for the approach and the other for the retraction

$$F(t) = \begin{cases} F_{bec}(t) & t \le t_{max} \\ F_{bec}(t_1) & t > t_{max} \end{cases} \quad (10)$$

where $t_1$ is defined as

$$t_1 = t - \sqrt[1-\gamma]{1 + \frac{v_{ret}}{v_{app}}}\,(t - t_{max}) \quad (11)$$

where $v_{app}$ and $v_{ret}$ are the velocities during approach and retraction. Complete expressions are found in the Supporting Information (Equations S7, S10, and S11, Supporting Information).

*Statistical Analysis*: The raw FDC curves were unfiltered. Hydrodynamic drag effects and baseline determination were performed as illustrated in Figure S5 and explained in the Supporting Information. To determine $E_0$ and $\gamma$ from a nanoindentation experiments, the FDCs were fitted with Equations S10 and S11, Supporting Information. For the nanorheology oscillatory experiments, the values of $E_0$ and $\gamma$ were obtained by using Equations 7 and 8. The values represented in Figure 2a,b,c were obtained using a sample size of $n = 72$. The values represented in Figure 2d,e,f were obtained using a sample size of $n = 36$. In Figure 4c–f, the sample size was of $n = 12$. In Figure 5, the sample size was of $n = 10$. In Figures 2, 3, 4 and 5 the dots represent the mean value, and the error-bars represent the standard deviation. The sample size refers to the number of curves.

## Supporting Information

Supporting Information is available from the Wiley Online Library or from the author.

## Acknowledgements

V.G.G. and F.M.E. contributed equally to this work. Financial support from the Ministerio de Ciencia e Innovación (PID2019-106801GB-I00 /AEI/10.13039/501100011033), CSIC 202050E013, Comunidad de Madrid S2018/NMT-4443 (Tec4Bio-CM) and the European Commission (HORIZON-EIC-2022, project Piezo4Spine, No. 101098597) are acknowledged.

## Conflict of Interest

The authors declare no conflict of interest.

## Data Availability Statement

The data that support the findings of this study are available from the corresponding author upon reasonable request.

## Keywords

atomic force microscopy (AFM), cell nanomechanics, mammalian cells, mechanobiology, nanoindentation, nanorheology

Received: June 9, 2023
Revised: September 1, 2023
Published online:

[1] O. Chaudhuri, J. Cooper-White, P. A. Janmey, D. J. Mooney, V. B. Shenoy, *Nature* **2020**, *584*, 535.
[2] A. Diz-Muñoz, O. D. Weiner, D. A. Fletcher, *Nat. Phys.* **2018**, *14*, 648.
[3] A. F. Girão, M. C. Serrano, A. Completo, P. A. A. P. Marques, *ACS Nano* **2022**, *16*, 13430.
[4] P.-H. Wu, D. R.-B. Aroush, A. Asnacios, W.-C. Chen, M. E. Dokukin, B. L. Doss, P. Durand-Smet, A. Ekpenyong, J. Guck, N. V. Guz, P. A. Janmey, J. S. H. Lee, N. M. Moore, A. Ott, Y.-C. Poh, R. Ros, M. Sander, I. Sokolov, J. R. Staunton, N. Wang, G. Whyte, D. Wirtz, *Nat. Methods* **2018**, *15*, 491.
[5] P. Roca-Cusachs, V. Conte, X. Trepat, *Nat. Cell Biol.* **2017**, *19*, 742.
[6] Y. M. Efremov, T. Okajima, A. Raman, *Soft Matter* **2020**, *16*, 64.
[7] R. Garcia, *Chem. Soc. Rev.* **2020**, *49*, 5850.
[8] N. Mandriota, C. Friedsam, J. A. Jones-Molina, K. V. Tatem, D. E. Ingber, O. Sahin, *Nat. Mater.* **2019**, *18*, 1071.
[9] C. R. Guerrero, P. D. Garcia, R. Garcia, *ACS Nano* **2019**, *13*, 9629.
[10] L. Stühn, A. Fritschen, J. Choy, M. Dehnert, C. Dietz, *Nanoscale* **2019**, *11*, 13089.
[11] M. Penedo, K. Miyazawa, N. Okano, H. Furusho, T. Ichikawa, M. S. Alam, K. Miyata, C. Nakamura, T. Fukuma, *Sci. Adv.* **2022**, *7*, eabj4990.
[12] Y. M. Efremov, D. M. Suter, P. S. Timashev, A. Raman, *Sci. Rep.* **2022**, *12*, 529.
[13] A. Rigato, A. Miyagi, S. Scheuring, F. Rico, *Nat. Phys.* **2017**, *13*, 771.
[14] G. Fläschner, C. I. Roman, N. Strohmeyer, D. Martinez-Martin, D. J. Müller, *Nat. Commun.* **2021**, *12*, 2922.
[15] X. Wang, H. Liu, M. Zhu, C. Cao, Z. Xu, Y. Tsatskis, K. Lau, C. Kuok, T. Filleter, H. Mcneill, C. A. Simmons, S. Hopyan, Y. Sun, *J. Cell Sci.* **2018**, *131*, jcs209627.
[16] D. Guan, E. Charlaix, R. Z. Qi, P. Tong, *Phys. Rev. Appl.* **2017**, *8*, 44010.
[17] M. Galluzzi, G. Tang, C. S. Biswas, J. Zhao, S. Chen, F. J. Stadler, *Nat. Commun.* **2018**, *9*, 3584.
[18] H. Schillers, C. Rianna, J. Schäpe, T. Luque, H. Doschke, M. Wälte, J. J. Uriarte, N. Campillo, G. P. A. Michanetzis, J. Bobrowska, A. Dumitru, E. T. Herruzo, S. Bovio, P. Parot, M. Galluzzi, A. Podestà, L. Puricelli, S. Scheuring, Y. Missirlis, R. Garcia, M. Odorico, J.-M. Teulon, F. Lafont, M. Lekka, F. Rico, A. Rigato, J.-L. Pellequer, H. Oberleithner, D. Navajas, M. Radmacher, *Sci. Rep.* **2017**, *7*, 5117.
[19] A. Marchesi, K. Umeda, T. Komekawa, T. Matsubara, H. Flechsig, T. Ando, S. Watanabe, N. Kodera, C. M. Franz, *Sci. Rep.* **2021**, *11*, 13003.
[20] P. D. Garcia, C. R. Guerrero, R. Garcia, *Nanoscale* **2017**, *9*, 12051.
[21] Y. M. Efremov, W.-H. Wang, S. D. Hardy, R. L. Geahlen, A. Raman, *Sci. Rep.* **2017**, *7*, 1541.
[22] Y. M. Efremov, A. I. Shpichka, S. L. Kotova, P. S. Timashev, *Soft Matter* **2019**, *15*, 5455.
[23] B. R. Brückner, H. Nöding, A. Janshoff, *Biophys. J.* **2017**, *112*, 724.
[24] J. S. De Sousa, J. A. C. Santos, E. B. Barros, L. M. R. Alencar, W. T. Cruz, M. V. Ramos, J. Mendes Filho, *J. Appl. Phys.* **2017**, *121*, 034901.
[25] F. B. De Sousa, P. K. V. Babu, M. Radmacher, C. L. N. Oliveira, J. S. De Sousa, *J Phys D Appl Phys* **2021**, *54*, 335401.
[26] A. Bonfanti, J. L. Kaplan, G. Charras, A. Kabla, *Soft Matter* **2020**, *16*, 6002.
[27] C. H. Parvini, A. X. Cartagena-Rivera, S. D. Solares, *Commun Biol* **2022**, *5*, 17.
[28] M. Mccraw, B. Uluutku, S. Solares, *Rep. Mech. Eng.* **2021**, *2*, 156.
[29] B. L. Doss, K. Rahmani Eliato, K.-H. Lin, R. Ros, *Soft Matter* **2019**, *15*, 1776.
[30] P. D. Garcia, R. Garcia, *Biophys. J.* **2018**, *114*, 2923.
[31] P. D. Garcia, R. Garcia, *Nanoscale* **2018**, *10*, 19799.
[32] P. D. Garcia, C. R. Guerrero, R. Garcia, *Nanoscale* **2020**, *12*, 9133.
[33] S. Moreno–Flores, R. Benitez, M. Vivanco, J. L. Toca–Herrera, *Nanotechnology* **2010**, *21*, 445101.
[34] D. A. D. Flormann, C. Anton, M. O. Pohland, Y. Bautz, K. Kaub, E. Terriac, T. E. Schäffer, J. Rheinlaender, A. Janshoff, A. Ott, F. Lautenschläger, *Front. Phys.* **2021**, *9*, 711860.
[35] S. V. Kontomaris, A. Stylianou, A. Georgakopoulos, A. Malamou, *Micron* **2023**, *164*, 103384.

[36] M. Krieg, G. Fläschner, D. Alsteens, B. M. Gaub, W. H. Roos, G. J. L. Wuite, H. E. Gaub, C. Gerber, Y. F. Dufrêne, D. J. Müller, *Nat. Rev. Phys.* **2019**, *1*, 41.
[37] G. Zhou, B. Zhang, G. Tang, X.-F. Yu, M. Galluzzi, *Adv Phys X* **2021**, *6*, 1866668.
[38] J. R. Ramos, J. Pabijan, R. Garcia, M. Lekka, *Beilstein J. Nanotechnol.* **2014**, *5*, 447.
[39] A. Calzado-Martín, M. Encinar, J. Tamayo, M. Calleja, A. San Paulo, *ACS Nano* **2016**, *10*, 3365.
[40] A. C. Dumitru, D. Mohammed, M. Maja, J. Yang, S. Verstraeten, A. Del Campo, M.-P. Mingeot-Leclercq, D. Tyteca, D. Alsteens, *Adv. Sci.* **2020**, *7*, 2002643.
[41] P. V. Kolluru, M. D. Eaton, D. W. Collinson, X. Cheng, D. E. Delgado, K. R. Shull, L. C. Brinson, *Macromolecules* **2018**, *51*, 8964.
[42] T. Niu, G. Cao, *RSC Adv.* **2014**, *4*, 29291.
[43] F. M. Hecht, J. Rheinlaender, N. Schierbaum, W. H. Goldmann, B. Fabry, T. E. Schäffer, *Soft Matter* **2015**, *11*, 4584.
[44] J. G. Sanchez, F. M. Espinosa, R. Miguez, R. Garcia, *Nanoscale* **2021**, *13*, 16339.
[45] M. Di Paola, A. Pirrotta, A. Valenza, *Mech. Mater.* **2011**, *43*, 799.
[46] E. H. Lee, J. R. M. Radok, *J Appl Mech* **1960**, *27*, 438.
[47] T. C. T. Ting, *J Appl Mech* **1968**, *35*, 248.
[48] B. Cappella, G. Dietler, *Surf. Sci. Rep.* **1999**, *34*, 1.
[49] J. Alcaraz, L. Buscemi, M. Grabulosa, X. Trepat, B. Fabry, R. Farré, D. Navajas, *Biophys. J.* **2003**, *84*, 2071.
[50] J. Alcaraz, L. Buscemi, M. Puig-De-Morales, J. Colchero, A. Baró, D. Navajas, *Langmuir* **2002**, *18*, 716.
[51] R. Liu, M. Roman, G. Yang, *Rev. Sci. Instrum.* **2010**, *81*, 063703.
[52] A. K. Denisin, B. L. Pruitt, *ACS Appl. Mater. Interfaces* **2016**, *8*, 21893.
[53] H. W. Wu, T. Kuhn, V. T. Moy, *Scanning* **1998**, *20*, 389.
[54] C. Rotsch, M. Radmacher, *Biophys. J.* **2000**, *78*, 520.
[55] V. S. Kolmogorov, A. S. Erofeev, E. Woodcock, Y. M. Efremov, A. P. Iakovlev, N. A. Savin, A. V. Alova, S. V. Lavrushkina, I. I. Kireev, A. O. Prelovskaya, E. V. Sviderskaya, D. Scaini, N. L. Klyachko, P. S. Timashev, Y. Takahashi, S. V. Salikhov, Y. N. Parkhomenko, A. G. Majouga, C. R. W. Edwards, P. Novak, Y. E. Korchev, P. V. Gorelkin, *Nanoscale* **2021**, *13*, 6558.
[56] I. Muntz, M. Fenu, G. J. V. M. Van Osch, G. H. Koenderink, *Phys Biol* **2022**, *19*, 021001.
[57] R. Oftadeh, B. K. Connizzo, H. T. Nia, C. Ortiz, A. J. Grodzinsky, *Acta Biomater.* **2018**, *70*, 249.
[58] J. R. Staunton, B. L. Doss, S. Lindsay, R. Ros, *Sci. Rep.* **2016**, *6*, 19686.
[59] M. L. Yubero, P. M. Kosaka, Á. San Paulo, M. Malumbres, M. Calleja, J. Tamayo, *Commun Biol* **2020**, *3*, 590.
[60] S. Hurst, B. E. Vos, M. Brandt, T. Betz, *Nat. Phys.* **2021**, *17*, 1270.